Completely flat bands and fully localized states on surfaces of anisotropic diamond-lattice models

Ryuji Takahashi[1,2] and Shuichi Murakami[1,3]

[1]*Department of Physics, Tokyo Institute of Technology, 2-12-1 Ookayama, Meguro-ku, Tokyo 152-8551, Japan*
[2]*Department of Applied Physics, University of Tokyo, 7-3-1 Hongo, Bunkyo-ku, Tokyo 113-8656, Japan*
[3]*TIES, Tokyo Institute of Technology, 2-12-1 Ookayama, Meguro-ku, Tokyo 152-8551, Japan*

(Dated: May 15, 2013)

We discuss flat-band surface states on the (111) surface in the tight-binding model with nearest-neighbor hopping on the diamond lattice, in analogy to the flat-band edge states in graphene with a zigzag edge. The bulk band is gapless, and the gap closes along a loop. The verge of the flat-band surface states is identical with this gap-closing loop projected onto the surface Brillouin zone. When anisotropies in the hopping integrals increase, the bulk gapless points move and the distribution of the flat-band states expands in the Brillouin zone. Then when the anisotropy is sufficiently large, the surface flat bands cover the whole Brillouin zone. Because of the completely flat bands, we can construct surface-state wavefunctions which is localized in all the three directions.

PACS numbers: 73.20.-r, 73.20.At, 73.22.Pr

I. INTRODUCTION

Flat bands have been studied particularly in the context of possible ferromagnetism driven by interactions, as was proposed by Lieb[1], and successively Mielke and Tasaki[2–5]. On the other hand, from the research on graphene[6] it is known that the tight-binding model with nearest-neighbor hopping on a honeycomb lattice with a zigzag edge exhibits flat-band edge states[7], and its origin is topologically interpreted[8]. In the dispersion of a graphene ribbon with zigzag edges, the flat bands appear between the wavenumbers corresponding to the projection of Dirac points at K and K'. In contrast, there is no flat band in the edge states in the graphene ribbon with armchair edges because in the projection of the dispersion, Dirac cones at K and K' overlap each other. In three-dimensions, the diamond lattice, i.e. a three-dimensional analogue of honeycomb lattice, exhibits flat-band surface states, as theoretically found in the nearest-neighbor tight-binding model[9].

When the hopping of the tight-binding model on the honeycomb lattice becomes anisotropic, the Dirac points in the bulk BZ move away from K and K'. Moreover when the tight-binding model has sufficiently large anisotropic hopping integrals, the two Dirac points meet and the bulk dispersion relation is linear in one direction and quadratic in the other[10]. In that case, the flat-band edge states cover the whole one-dimensional (1D) BZ[11]. With the increase of the anisotropy, the bulk becomes gapped while the complete flat band remains tn the edge BZ.

In this paper we focus on surface flat bands in the tight-binding models on the diamond lattices with (111) surface. When the model has no anisotropy, the gap closes along a loop in the bulk BZ. If the Fermi energy is set to be zero, which corresponds to the case with particle-hole symmetry, the bulk Fermi surface (FS) coincides with this loop. An anisotropy in the nearest-neighbor hopping integrals deforms the loop. Similarly to the honeycomb-lattice model, the surface flat bands are formed in the $\mathbf{k}$ region surrounded by the projection of the FS loop. When the anisotropy is sufficiently large, the FS loop vanishes, and consequently the flat-band surface states cover the whole 2D BZ.

Furthermore, because the edge/surface band is completely flat over the entire BZ in the models on honeycomb/diamond lattices, any linear combinations of the edge/surface states remains eigenstates. Thereby we can construct the edge/surface states which are spatially localized in all directions. In the diamond-lattice model we also find a topological transition of the bulk FS by changing anisotropy; the loop of the bulk FS changes its topology by varying the hopping integrals.

The organization of the paper is as follows. In Sec. II we review how the flat-band edge states of the tight-binding model on the honeycomb lattice evolve as we change an anisotropy. We discuss analogous behaviors of surface states of the model on the diamond lattice in Sec. III. In Sec. IV, we show how the behaviors of the edge/surface states shown so far are explained by topological argument. Section V is devoted to a calculation of the states which is localized along the boundary, for both the honeycomb- and diamond-lattice models. We summarize our results in Sec. VI.

II. HONEYCOMB LATTICE

We first review the flat-band edge states on the honeycomb-lattice structure shown in Fig. 1(a), and study the completely flat band, which has been studied in Ref. 11. We consider a tight-binding Hamiltonian on

this lattice,

$$H_{\rm h} = \sum_{\langle ij \rangle} c_i^\dagger t_{ij} c_j, \tag{1}$$

where the suffix h represents the honeycomb lattice, t_{ij} is the hopping integral along the nearest-neighbor bond vector $\boldsymbol{\tau}_a$, and c_i ($c_i^\dagger$) is the annihilation (creation) operator of the electron. We treat the hopping integrals t_{ij} as real positive parameters, and they are labeled with the vectors $\boldsymbol{\tau}_a$ as t_a. The bulk Hamiltonian matrix $H_{\rm hb}(\mathbf{k})$ at wavevector $\mathbf{k}$ is given as

$$H_{\rm hb}(\mathbf{k}) = \begin{pmatrix} 0 & \sum_{i=1}^3 t_i {\rm e}^{-i\mathbf{k}\cdot\boldsymbol{\tau}_i} \\ \sum_{i=1}^3 t_i {\rm e}^{i\mathbf{k}\cdot\boldsymbol{\tau}_i} & 0 \end{pmatrix}. \tag{2}$$

where the suffix b means the bulk. $\boldsymbol{\tau}_{i=1,2,3}$ are expressed as $\boldsymbol{\tau}_1 = (0,1), \boldsymbol{\tau}_2 = (-\frac{\sqrt{3}}{2}, -\frac{1}{2}), \boldsymbol{\tau}_3 = (\frac{\sqrt{3}}{2}, -\frac{1}{2})$, where we put the length of the nearest-neighbor bonds as unity. For simplicity t_i are assumed to be positive. The primitive vectors $\mathbf{a}_{i=1,2}$ are $\mathbf{a}_1 = (\frac{\sqrt{3}}{2}, \frac{3}{2}), \mathbf{a}_2 = (-\frac{\sqrt{3}}{2}, \frac{3}{2})$. The reciprocal primitive vectors are $\mathbf{G}_1 = 2\pi\frac{2}{3}(\frac{\sqrt{3}}{2}, \frac{1}{2}), \mathbf{G}_2 = 2\pi\frac{2}{3}(-\frac{\sqrt{3}}{2}, \frac{1}{2})$.

We first note that the bulk Hamiltonian $H_{\rm hb}$ has particle-hole symmetry: $\sigma_3 H_{\rm hb}\sigma_3 = -H_{\rm hb}$. Therefore, if $|\psi\rangle$ is an eigenstate with the eigenvalue E, $\sigma_3|\psi\rangle$ is an eigenstate with energy $-E$. The eignenvalue is given by

$$E_{\rm hb}(\mathbf{k}) = \pm \left| t_i \sum_{i=1}^3 {\rm e}^{-i\boldsymbol{\tau}_i\cdot\mathbf{k}} \right|. \tag{3}$$

Hereafter we put parameters $t_2 = t_3 = 1$, and $t_1 = t$, where t is a real positive tunable parameter. The bulk dispersion is given as

$$E_{\rm hb}^2 = \left(t + 2\cos\frac{\sqrt{3}k_x}{2}\cos\frac{3k_y}{2} \right)^2 + 4\cos^2\frac{\sqrt{3}k_x}{2}\sin^2\frac{3k_y}{2} \tag{4}$$

The bulk gapless points (k_x^*, k_y^*) are given by the equations: $\cos\frac{\sqrt{3}k_x^*}{2} = \pm\frac{1}{2}t$ and $\sin\frac{3}{2}k_y^* = 0$. The equations give two gapless points in the bulk BZ, and they exist for $t \leq 2$. The gapless points move with the change of the anisotropy t. For $t = 1$, i.e. the tight-binding model of graphene, the upper and lower bands touch at K ($\frac{2\pi\sqrt{3}}{9}, \frac{2\pi}{3}$) and K' ($-\frac{2\pi\sqrt{3}}{9}, \frac{2\pi}{3}$), and with the increase of t the gapless points get closer along the line $k_y = \frac{2\pi}{3}$ (Fig. 1(b)). Around each of the two gapless points, the dispersion forms a Dirac cone, and Berry phase around each gapless point is π. Because of this π Berry phase, the gapless points do not disappear as we change $t(< 2)$. The bulk gapless points move in the direction perpendicular to the anisotropic hopping integral t. At $t = 2$ the gapless points meet and they annihilate each other at $k_x = 0$ (Fig. 1(b))[10]. For $t > 2$, there are no bulk gapless points.

The evolution of the edge states with the change of the anisotropy has been studied in several papers[10–12]. As we see in the following, for $t > 2$ flat-band edge states on the zigzag or Klein edges completely cover the BZ[11]. It occurs when the bond with hopping t is perpendicular to the edge for the zigzag edges, or when the bond with hopping t is not perpendicular to the edge for the Klein edges. We calculate dispersions in Fig. 1 (c) for $t_1 = 1$ and $t_1 = 2.2$, $t_2 = t_3 = 1$. The flat-band edge states are separated completely from the bulk for $t_1 = 2.2$ (Fig. 1(c)). To explain this behavior, we solve the Schrödinger equation in the semi-infinite geometry with a zigzag boundary. The zigzag edge is assumed to be perpendicular to the bonds with hopping integral t_1. We express the wavefunction $|\Psi(k)\rangle$ as

$$|\Psi(k)\rangle = \sum_{i=1} (a_i(k)|A_i(k)\rangle + b_i(k)|B_i(k)\rangle), \tag{5}$$

where i denotes the index for unit cells containing two sublattices, A and B, counted from the edge ($i = 1$), k is the wavenumber along the edge, and $a_i(k)$ ($b_i(k)$) denotes the amplitude of the Bloch wavefunctions $|A_i(k)\rangle$ ($|B_i(k)\rangle$) for the i-th A (B) sublattice. Acting $H_{\rm h}$ onto $|A_i(k)\rangle$ and $|B_i(k)\rangle$, we have

$$\langle B_i(k)|H_{\rm h}|A_i(k)\rangle = t_1, \tag{6}$$

$$\langle B_{i-1}(k)|H_{\rm h}|A_i(k)\rangle = t_2 + t_3{\rm e}^{-ik}. \tag{7}$$

When the eigenvalue is zero, $H_{\rm h}|\Psi(k)\rangle = 0$, we obtain

$$a_i(t_2 + t_3{\rm e}^{-ik}) + a_{i+1}t_1 = 0, \;\; b_i = 0. \tag{8}$$

Thus the condition for existence of the edge states, i.e. normalizability of the wavefunction, is given as

$$\left| \frac{t_2 + t_3{\rm e}^{-ik}}{t_1} \right| < 1, \tag{9}$$

and we have the amplitude of the flat-band states as

$$a_n(k) = a_1 \left[-\frac{t_2 + t_3{\rm e}^{-ik}}{t_1} \right]^{n-1}, \;\; b_i = 0 \tag{10}$$

where $a_1 = \left[1 - \frac{|t_2 + t_3{\rm e}^{-ik}|^2}{t_1^2}\right]^{-1/2}$ from normalization. For $t_1 = t_2 = t_3$ (graphene model), the wavenumber which satisfies the condition (Eq. (9)) for existence of the edge state is given as $\frac{2\pi}{3} < k < \frac{4\pi}{3}$, which agrees with the well-known flat band in graphene ribbon with a zigzag edge[7]. In addition, by the relation $\left|\frac{t_2+t_3{\rm e}^{-ik}}{t_1}\right| < \frac{t_2+t_3}{t_1}$, the flat bands cover the whole 1D BZ when $t_1 > t_2 + t_3$ is satisfied. This is realized when anisotropy is sufficiently large. These results agree with numerical calculations in Fig. 1 (c). In Fig. 1 (c) we also show results for armchair edges and for Klein (bearded) edges. For armchair edges there are no flat-band edge states, For Klein edges where τ_1-bonds (hopping t_1) are not perpendicular to the edge, there are flat-band edge states; if $t_1 > 2$ the flat-band edge states cover the entire BZ. These results agree with the results in Ref. 11.

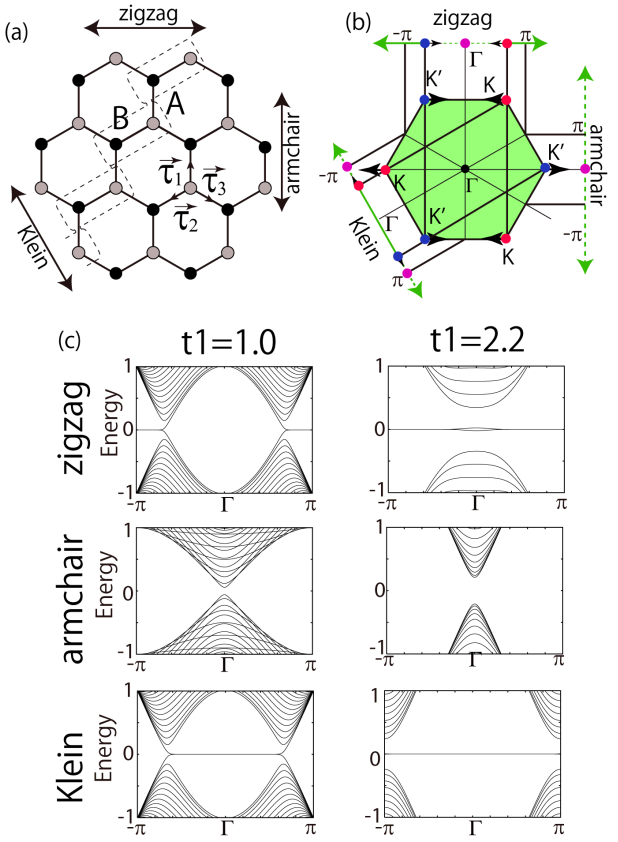

FIG. 1: (a) Schematic of the honeycomb-lattice structure. The dotted line shows a choice of unit cell with translational symmetry along the edge. The arrows show the directions along zigzag, armchair, and Klein edges. (b) shows the first BZ of the honeycomb lattice. Dots at the corners show the gapless points. The bulk bands become gapless at K and K' points, when the hopping integral is isotropic. By increasing t_1 from $t_2 = t_3 = 1$, the gapless points move away from K and K' points as shown by the arrows. The flat-band edge states expand in the BZ as the bulk gapless points move. (c) shows the dispersions for $t_1 = 1$ and 2.2 at $t_2 = t_3 = 1$. The dispersions are shown for zigzag, armchair and Klein edges. In zigzag and Klein edges, flat bands appear at the Fermi energy.

III. DIAMOND LATTICE

In the previous section, we have seen that the flat band of the honeycomb lattice with the large anisotropy covers the whole edge BZ. In this section we show surface flat bands[9] in the tight-binding model of the diamond lattice in the same method in the previous model on the honeycomb lattice. In the honeycomb lattice, the verge of the flat bands is identified with the bulk gapless points. We will show the same phenomena for the diamond lattice. The Hamiltonian $H_{\rm d}$ is

$$H_{\rm d} = \sum_{\langle ij \rangle} c_i^\dagger t_{ij} c_j, \tag{11}$$

where $t_{ij} = t_{ji}$ is the hopping integral from site i to j, and the suffix d means the diamond lattice. We assume that the hopping integrals are real positive parameters. The nearest-neightbor bond vectors, $\boldsymbol{\tau}$s, are as follows: $\boldsymbol{\tau}_1 = \frac{1}{4}(1,1,1)$, $\boldsymbol{\tau}_2 = \frac{1}{4}(-1,1,-1)$, $\boldsymbol{\tau}_3 = \frac{1}{4}(-1,-1,1)$, and $\boldsymbol{\tau}_4 = \frac{1}{4}(1,-1,-1)$ (Fig. 2). The hopping integrals

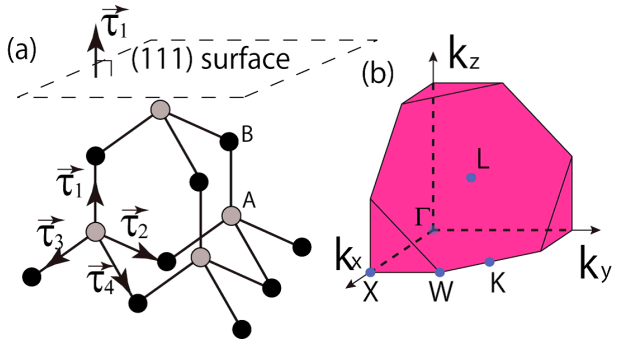

FIG. 2: (a) Schematic of a diamond lattice. A (gray) and B (black) atoms denote the sublattice. $\boldsymbol{\tau}$s represent vectors connecting nearest-neighbor atoms. (b) The BZ of the diamond lattice structure within $k_{x,y,z} > 0$.

are labeled with $\boldsymbol{\tau}_a$ as $t_{\boldsymbol{\tau}_a} = t_a$. The bulk Hamiltonian $H_{\rm db}(\mathbf{k})$ is represented as

$$H_{\rm db}(\mathbf{k}) = \begin{pmatrix} 0 & \sum_{i=1}^4 t_i e^{-i\mathbf{k}\cdot\boldsymbol{\tau}_i} \\ \sum_{i=1}^4 t_i e^{i\mathbf{k}\cdot\boldsymbol{\tau}_i} & 0 \end{pmatrix}. \tag{12}$$

This also satisfies $\sigma_3 H_{\rm db} \sigma_3 = -H_{\rm db}$, and therefore the eigenstates have particle-hole symmetry. As is proposed in 9, when t_i's are identical, the surface states on the (111) surface for this Hamiltonian forms a flat band, which partially cover the surface BZ.

First, we set one of the four hopping integrals as a tunable positive parameter t and the other hopping integrals as unity. For $t = 1.4$, the dispersions for slab geometry with (111) surface are shown in Fig. 3(a)(b). In Fig. 3(a) we set $t_1 = t$, $t_2 = t_3 = t_4 = 1$ and in Fig. 3(b) we set $t_3 = t$, $t_1 = t_2 = t_4 = 1$. The left panels of Fig. 3(a)(b) show the dispersions near zero energy, and the distributions of zero-energy flat bands in the surface BZ are shown in the right panels in (a)(b). Fig. 3(c) shows the projections of the bulk FS ($E = 0$) onto the (111) surface for (a)(b). By comparing the FSs in Fig. 3(c) with the flat-band states (a)(b), we see the correspondence between the bulk FS and the distribution of the flat bands as is discussed in the previous case of the honeycomb lattice; the verge of the flat bands corresponds to the bulk FS projected onto the surface direction. The bulk FS forms a loop in the bulk BZ because $H_{\rm db}$ consists only of σ_x and σ_y. In this case, the FS loop encircles the axis parallel to the hopping vector with the hopping integral t. Therefore by rotating the surface orientation in (b) from (111) to $(\bar{1}\bar{1}1)$, the bulk FS is rotated as well, and correspondingly we have the same flat-band states as shown in (a).

The bulk dispersion for $t_1 = t$, $t_2 = t_3 = t_4 = 1$ is given by

$$E_{\rm db}^2 = \left|\sum_{i=1}^{4} t_i e^{-i\mathbf{k}\cdot\boldsymbol{\tau}_i}\right|^2 = \left(t + \cos\frac{k_x+k_y}{2} + \cos\frac{k_y+k_z}{2} + \cos\frac{k_z+k_x}{2}\right)^2 + \left(\sin\frac{k_x+k_y}{2} + \sin\frac{k_y+k_z}{2} + \sin\frac{k_z+k_x}{2}\right)^2 \quad (13)$$

Therefore, the gapless points $E_{bd} = 0$ are given by two equations, $t + \cos\frac{k_x+k_y}{2} + \cos\frac{k_y+k_z}{2} + \cos\frac{k_z+k_x}{2} = 0$ and $\sin\frac{k_x+k_y}{2} + \sin\frac{k_y+k_z}{2} + \sin\frac{k_z+k_x}{2} = 0$ which determine the bulk FS are shown in Fig. 4. The FS encircles the Γ-L line in the bulk BZ for $t \geq 1$. We see that the FS is getting smaller with the increase of t_1 and shrinks to the Γ point at $t = 3$, while the flat-band surface states expand with the increase of t_1. For $t > 3$ the loop vanishes, and the surface flat band covers the whole surface BZ.

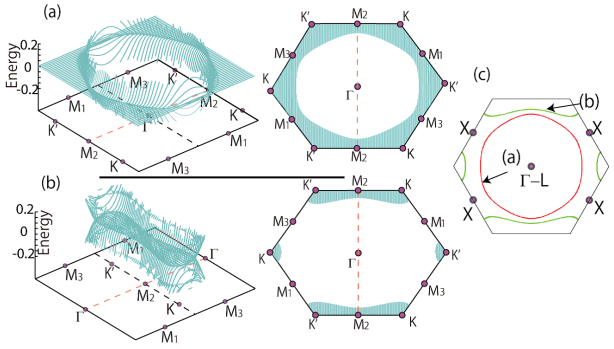

FIG. 3: Band structure for the diamond lattice model with the (111) surface, for $t_2 = t_4 = 1$ and (a) $t_1 = 1.4$ and $t_3 = 1$ or (b) $t_1 = 1$ and $t_3 = 1.4$. The right panels in (a)(b) show the region with the surface flat bands. In (c), the FS ($E_{bd} = 0$) in the 3D bulk BZ projected on the (111) plane for the cases (a) and (b).

A. Flat-band states localized at the surface

Here we show the Bloch wavefunction of the flat-band states for the tight-binding model (Eq. (11)) with a (111) surface. To this end, we consider the tight-binding model on a semi-infinite geometry of the diamond lattice with the (111) surface. We derive a wavefunction with zero eigenvalue as $|\phi\rangle = \sum_{i=1}(a_i(\mathbf{k})|A_i(\mathbf{k})\rangle + b_i(\mathbf{k})|B_i(\mathbf{k})\rangle)$, where i denotes indices of the unit cell containing A and B sublattice sites, counted from the top ($i = 1$), and $a_i(\mathbf{k})(b_i(\mathbf{k}))$ denotes the amplitude of the Bloch wavefunction for each sublattice. The matrix element of the Hamiltonian $H_{\rm d}$ is given as

$$\langle B_{j-1}(\mathbf{k})|H_{\rm d}|A_j(\mathbf{k})\rangle = t_1, \quad (14)$$

$$\langle B_j(\mathbf{k})|H_{\rm d}|A_j(\mathbf{k})\rangle = t_2 e^{-ik_1} + t_3 + t_4 e^{ik_2}, \quad (15)$$

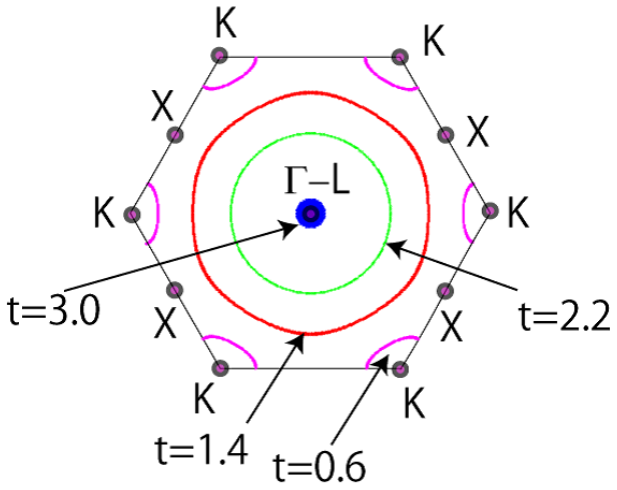

FIG. 4: The FS ($E_{bd} = 0$) in the 3D bulk BZ projected on the (111) plane for $t_2 = t_3 = t_4 = 1$ and $t_1 = 0.6, 1.4, 2.2, 3.0$ are shown. For $t_1 > 1$, the loop shrinks with increase in t_1, and at $t_1 = 3.0$ the loop becomes a dot.

where $k_1 = \mathbf{k}\cdot(\boldsymbol{\tau}_2 - \boldsymbol{\tau}_3)$ and $k_2 = \mathbf{k}\cdot(\boldsymbol{\tau}_3 - \boldsymbol{\tau}_4)$. In the Schrödinger equation, $H_{\rm d}|\phi\rangle$ can be calculated as

$$H_{\rm d}|\phi(\mathbf{k})\rangle = \sum_{j=2}^{\infty}[a_j(t_2 e^{-ik_1} + t_3 + t_4 e^{ik_2}) + a_{j+1}t_1]|B_j(\mathbf{k})\rangle + [b_1(t_2 e^{-ik_1} + t_3 + t_4 e^{ik_2})]|A_1(\mathbf{k})\rangle + \sum_{j=2}^{\infty}[b_{j-1}t_1 + b_j(t_2 e^{ik_1} + t_3 + t_4 e^{-ik_2})]|A_j(\mathbf{k})\rangle \quad (16)$$

From $H_{\rm d}|\phi\rangle = 0$, the amplitudes are derived as $b_i(k) = 0$, and

$$a_{j+1}(\mathbf{k}) = -\frac{t_2 e^{-ik_1} + t_3 + t_4 e^{ik_2}}{t_1} a_j(\mathbf{k}). \quad (17)$$

Namely, the zero-energy states localize near the surface for every wavenumber for $t_1 > t_2 + t_3 + t_4$, because we have

$$\left|\frac{a_{j+1}(\mathbf{k})}{a_j(\mathbf{k})}\right| = \left|\frac{t_2 e^{-ik_1} + t_3 + t_4 e^{ik_2}}{t_1}\right| \leq \frac{(t_2 + t_3 + t_4)}{t_1} < 1 \quad (18)$$

from Eq. (17). The second equality in Eq. (18) holds only at the Γ point in the 2D surface BZ. In addition, from Eq. (18) a penetration depth λ, defined as $|a_j| \sim e^{-j/\lambda}$, is calculated for each $\mathbf{k}$. Equation (18) gives $e^{-\frac{1}{\lambda}} = \left|\frac{t_2 e^{-ik_1} + t_3 + t_4 e^{ik_2}}{t_1}\right|$. Hence the penetration depth of the surface states is maximum at $\mathbf{k} = 0$, and the finite-size effect is the largest.

From the above discussion, the model can have the complete flat band at zero energy when the system is semi-infinite. However, if the thickness of the slab is finite, there is a small gap around the Γ point, as shown

in our numerical results for surface-state dispersions in Fig. 5(a)(b). The maximum value of the finite-size gap Λ is estimated as the following. We focus on the Γ point, and assume $(t_2+t_3+t_4)/t_1 = \alpha < 1$. When the thickness of the slab N is large, the surface wavefunction for the top surface $|\phi^t\rangle$ and that for the bottom surface $|\phi^b\rangle$ can be treated separately. The wavefunctions are approximately given as

$$|\phi^t(\mathbf{k})\rangle \sim \sum_{n=1}^{N} ac^{n-1}|A_i(\mathbf{k})\rangle,\ |\phi^b(\mathbf{k})\rangle \sim \sum_{n=1}^{N} ac^{N-n}|B_i(\mathbf{k})\rangle, \quad (19)$$

where $c = -(t_2 e^{-ik_1} + t_3 + t_4 e^{ik_2})/t_1$, and $a^2 = (1-|c|^2)/(1-|c|^{2N})$. Then we obtain the hybridization as

$$\langle\phi^b(\mathbf{k})|H|\phi^t(\mathbf{k})\rangle \sim a^2 c^N t_1, \quad (20)$$

which is expected to give the size of the gap due to the finite-size effect. At the Γ point, $|c|$ becomes maximum and therefore the finite-size effect of the energy is largest at Γ, taking its maximum value

$$\Lambda \sim t_1(1-\alpha^2)\alpha^N \quad (21)$$

For $t_1 = 3.4$, $t_2 = t_3 = t_4 = 1.0$, $t_1\alpha^N \sim 0.0616$ for $N = 20$, and $t_1\alpha^N \sim 0.00504$ for $N = 40$. Our band-structure calculation gives Λ to be $\Lambda \sim 0.0632$ for $N = 20$, and $\Lambda = 0.005042$ for $N = 40$, as shown in Fig. 5. Thus our estimate for λ in Eq. (21) well agrees with numerical calculation.

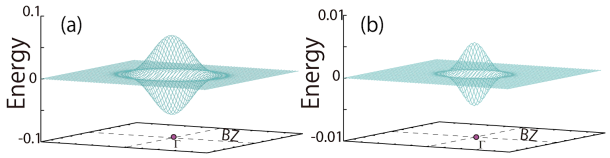

FIG. 5: Surface dispersion near the Fermi energy at $t = 3.4$. The number N of unit cells to the direction normal to the surface is $N = 20$ in (a) and $N = 40$ in (b). The surface BZ is the same as that in the left panel of the Fig. 3(a).

B. Topological transition of the bulk FS

In this section, a topological transition of the FS in the diamond lattice is discussed. We assume that $t_{2,3,4}$ are fixed to be unity, whereas $t_1 = t$ is varied. To illustrate the change of topology of the FS, we choose the scheme of the BZ as shown in Fig. 6. For $t < 1$ the FS is separated in the BZ. The Fermi loop reaches the boundary of the BZ, and forms an open orbit. On the other hand, for $t > 1$, the loop is connected in one closed loop in the BZ, and the FS shrinks with an increase of t. The transition of the topology of the FS occurs at $t = 1$. The FSs for $t = 0.8, 1, 1.2$ are plotted in Fig. 6 to show the process of the transition. In the figure the BZ is shown as the dotted line, and the straight lines shows the FS at $t = 1$: $k_x = \pm 2\pi$ or $k_y = \pm 2\pi$ at $k_z = 0$, $k_x = 2\pi$ at $k_y = 0$ and $k_y = 2\pi$ at $k_x = 0$. The squares at $k_z = 0$ and 2π are equivalent. At $t = 3$ the FS shrinks to a point and simultaneously the surface flat band extends cover the whole BZ.

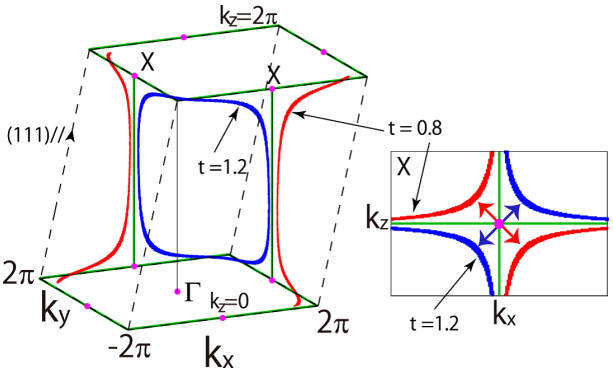

FIG. 6: The FSs in the 3D bulk BZ for $t_2 = t_3 = t_4 = 1$ and t_1 =0.8, 1, 1.2 are shown. At t_1 =0.8 the FS is separated in the BZ. On the other hand at $t_1 = 1.2$, the FS becomes one closed loop in the BZ. The topological transition occurs at $t_1 = 1$. At the right side, the FSs around the X point are magnified. The change in FS topology occurs at the X point.

IV. TOPOLOGICAL EXPLANATION FOR EXISTENCE OF THE FLAT-BAND STATES

Here we give a topological reason for existence of the flat-band edge/surface states in the present models, based on Ref. 8. For the honeycomb-lattice model, for example, we first begin with a bulk system, and later we cut the system along one direction by cutting the nearest-neighbor bonds, in order to discuss edge states. Let y denote the coordinate along which the system will be cut. Then, following Ref. 8, we expand the bulk Hamiltonian by the Pauli matrices $\sigma_{x,y}$ as $H = h_x(k'_x, k_y)\sigma_x + h_y(k'_x, k_y)\sigma_y$. Here k_y denotes the component of the wavevector along the y-direction (along the edge), and k'_x is another component of the wavevector. If the bulk system is cut along the y-axis, k'_x will no longer be a good quantum number. Then the criterion in Ref. 8 says that if the trajectory of (h_x, h_y) for the change of k'_x with fixed k_y encircles the origin, zero-energy edge states exist for the given k_y. If not, zero-energy edge states will not exist[8].

We apply this criterion to the present models to show that the flat-band boundary states discussed so far are fully explained by this theory. For the anisotropic honeycomb-lattice models, explanations are given in Ref. 11. For zigzag edges we have

$$h_x = t\cos(k_y - k'_x) + 1 + \cos k_y, \quad (22)$$
$$h_y = -t\sin(k_y - k'_x) + \sin k_y. \quad (23)$$

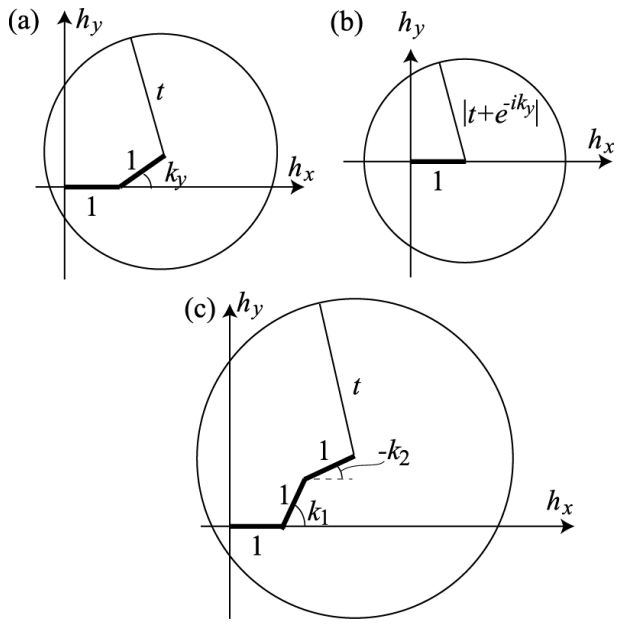

FIG. 7: Trajectories of (h_x, h_y) for the honeycomb-lattice model with zigzag (a), with Klein (b) edges, and in the diamond-lattice model with the (111) surface (c). In these trajectories k_y, k_1 and k_2 are fixed while k'_x and k_3 are changed.

Hence the trajectory is a circle with a radius $|t|$ centered at $(1+\cos k_y, \sin k_y)$ (Fig. 7(a)). The condition that it encircles the origin fully reproduce the behavior of the flat-band edge states. In particular, for $t > 2$ the trajectory encompasses the origin irrespective of the value of k_y, and existence of the perfectly flat band results. The case for the Klein edge is explained similarly, where we have

$$h_x = 1 + \cos(k_y - k'_x) + t\cos k'_x, \tag{24}$$
$$h_y = -\sin(k_y - k'_x) + t\sin k'_x. \tag{25}$$

with the trajectory shown in Fig. 7(b). The flat-band edge states extend over the whole BZ when $t > 2$.

Moreover, this discussion can be extended to three-dimensional model such as our diamond-lattice model.

$$h_x = 1 + \cos k_1 + \cos k_2 + t\cos k_3, \tag{26}$$
$$h_y = \sin k_1 - \sin k_2 - t\sin k_3, \tag{27}$$

where $k_1 = \mathbf{k}\cdot(\boldsymbol{\tau}_2 - \boldsymbol{\tau}_3)$, $k_2 = \mathbf{k}\cdot(\boldsymbol{\tau}_3 - \boldsymbol{\tau}_4)$, and $k_3 = \mathbf{k}\cdot(\boldsymbol{\tau}_3 - \boldsymbol{\tau}_1)$. When we cut the bonds parallel to $\boldsymbol{\tau}_1$, k_3 will no longer be a good quantum number. Then, if the trajectory of (h_x, h_y) by the change of k_3 encircles the origin, there should be zero-energy edge state. For $t > 3$ it holds true irrespective of the values of k_1 and k_2, and therefore the surface flat band covers the surface BZ (Fig. 7(c)).

This explanation also implies that in these models, the verge of the edge/surface states should be identical with the projection of bulk FS where the conduction and valence bands touch each other. Let $\mathbf{k}^*$ denote a wavenumber where the bulk FS satisfies $h_x = 0$ and $h_y = 0$. In our case the honeycomb lattice model has two $\mathbf{k}^*$ points (Fig. 1). $\mathbf{k}^*$ in the diamond lattice model forms a loop (Fig. 3 and 4). Their projections onto the edge/surface are identical with the verge of the flat-band edge/surface states, which is one of the consequences in Ref. 8. Thus this topological notion enables us to show existence or absence of flat-band boundary states for various boundary conditions. When the flat-band edge/surface states exist, the region enclosed by $\mathbf{k}^*$ varies by changing anisotropy of the hopping integral.

V. COMPLETELY LOCALIZED EDGE/SURFACE STATES

We have found that tight-binding models on the bipartite lattices, such as honeycomb and diamond lattices, have flat-band boundary states covering the whole BZ, when the anisotropy of their hopping integrals is sufficiently large. In general when systems have completely flat bands, one can construct a wavefunction which is spatially localized on a finite number of sites, as schematically shown in Fig. 8. It is possible only when the flat band covers the whole BZ. In this section, we show the localized wavefunction in the present models. This wavefunction is exponentially decaying in the direction normal to the boundary, while on the outermost atomic layer, the wavefunction is nonzero only on a single site. We consider semi-infinite systems for the honeycomb lattice with the zigzag edge and those for the diamond lattice with the (111) surface, and similarly to the previous sections, the A sublattice faces the boundary.

We first consider the honeycomb lattice in the half plane $y \le 0$. The zigzag edge is along the x axis, and the origin $\mathcal{O}$ is set to be one site on the zigzag edge. The state at the site $-m\mathbf{a}_1 - n\mathbf{a}_2$ is denoted as $|A_{mn}\rangle$ where $\mathbf{m} = (m, n)$ are integers, and $\mathcal{O} = (0, 0)$. We assume that for the flat-band state the wavefunction at the boundary states is nonzero only at $\mathcal{O}$. We express the wavefunction of the flat-band states as

$$|\Psi\rangle = \sum_{m,n} a_{mn}|A_{mn}\rangle, \tag{28}$$

where a_{mn} is the amplitude for $|A_{mn}\rangle$. From the Schrödinger equation, we have the relations between amplitudes as

$$t_1 a_{mn} + t_2 a_{m-1n} + t_3 a_{mn-1} = 0. \tag{29}$$

Intriguingly the solution of the above sequence is the same as the following problem. Consider a mover in the xy plane on the grid (Fig. 9). The mover is first on the $O = (0, 0)$ site. At each step it moves by $(1, 0)$ with a probability P_1, by $(0, 1)$ with a probability P_2 (Fig. 9), and the movement is finished otherwise. Finally after $N = m + n$ steps the probability P_{mn} that the mover is

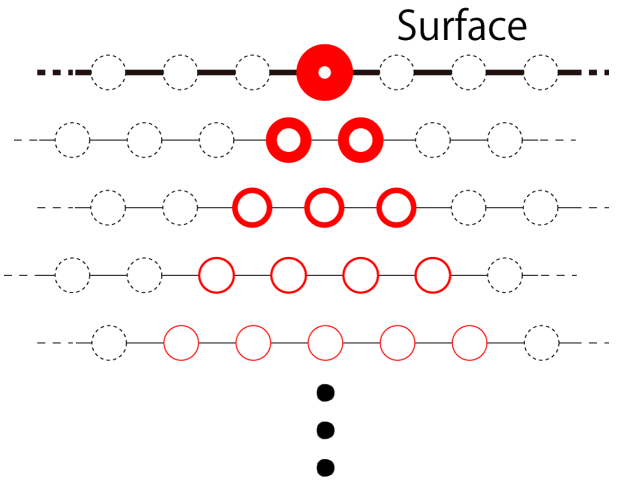

FIG. 8: Schematic of spatial distribution of the flat-band surface states. The circles are the A sublattices, while the amplitudes on B sublattices are zero and are omitted. The dotted circles show that their amplitudes of the wavefunction are zero. The line thickness of the circle shows the magnitude of the amplitude. The top atom has the largest amplitude, and the distribution of the wavefunction spatially spreads toward the interior with exponential decay. This picture of the fully localized states are in common with the honeycomb lattice with a zigzag edge and the diamond lattice with the (111) surface.

on (m,n) $(m,n\geq 0)$ along the shortest path is given as

$$P_{mn}=\frac{(m+n)!}{m!n!}P_1^m P_2^n. \tag{30}$$

By replacing the probabilities of the movement with the ratio of the hopping integrals,

$$P_i \to -\frac{t_{i+1}}{t_1}, \tag{31}$$

where $i=1,2$, we have the amplitude of the wavefunction as

$$a_{mn}=\frac{1}{Z_{\rm h}}\frac{(m+n)!}{m!n!}\left(-\frac{t_2}{t_1}\right)^m\left(-\frac{t_3}{t_1}\right)^n \quad (m,n\geq 0), \tag{32}$$

where $Z_{\rm h}$ is the normalization constant. For $m<0$ or $n<0$, a_{mn} vanishes. In this spatial representation of the wavefunction, the condition for the existence of the localized states on the boundary is that the wavefunction is normalizable. Generally, when $t_{1,2,3}(>0)$ are independnt parameters, $Z_{\rm h}$ satisfies the following relation:

$$\begin{aligned} Z_{\rm h}^2 &= \sum_{N=0}^{\infty}\sum_{n,m=0}^{N}\delta_{n+m,N}P_{mn}^2 \\ &\leq \left(\sum_{N=0}^{\infty}\sum_{n,m=0}^{N=n+m}|P_{mn}|\right)^2 = \left[\sum_{N=0}^{\infty}\left(\frac{t_2+t_3}{t_1}\right)^N\right]^2 \end{aligned} \tag{33}$$

Therefore for $\frac{t_2+t_3}{t_1}<1$, the renormalization constant $Z_{\rm h}$ converges; namely the completely flat-band states appear.

Next we consider the diamond lattice with the (111) surface in the half space $x+y+z\leq 0$. The surface are located on $x+y+z=0$ plane, and the origin $\mathcal{O}$ is set to be $(0,0,0)$. The wavefunction at $m\mathbf{d}_1+n\mathbf{d}_2+k\mathbf{d}_3$ is denoted as $|A_{mnk}\rangle$, where $\mathbf{d}_i=\boldsymbol{\tau}_{i+1}-\boldsymbol{\tau}_1$ for $i=2,3,4$. Then, the wavefunction of the flat-band state localized on the origin is denoted as

$$|\Psi\rangle=\sum_{m,n,k}a_{mnk}|A_{mnk}\rangle, \tag{34}$$

where a_{mnk} is the amplitude for $|A_{mn}\rangle$. By the Schrödinger equation, we have the relations between amplitudes as

$$t_1 a_{mnk}+t_2 a_{m-1nk}+t_3 a_{mn-1k}+t_4 a_{mnk-1}=0 \tag{35}$$

Similarly to the case of the honyecomb lattice, the solution for the sequence is obtained by the shortest path problem in 3D. let P_1, P_2 and P_3 denote the probabilities for moving along $(1,0,0)$, $(0,1,0)$ and $(0,0,1)$ respectively. The probability P_{mnk} of the shortest path problem from O to (m,n,k) is given as

$$P_{mnk}=\frac{(m+n+k)!}{m!n!k!}P_1^m P_2^n P_3^k. \tag{36}$$

By replacing the probabilities of the movement with the ratio of the hopping integrals, we have the amplitude a_{mnk} as

$$a_{mnk}=\frac{1}{Z_{\rm d}}\frac{(m+n+k)!}{m!n!k!}\left(-\frac{t_2}{t_1}\right)^m\left(-\frac{t_3}{t_1}\right)^n\left(-\frac{t_4}{t_1}\right)^k \tag{37}$$

where $Z_{\rm d}$ is the normalization constant for the wavefunction $|\Psi\rangle$, and this amplitude is nonzero only when m, n, k are all nonnegative. The condition for the existence of the flat-band is that $Z_{\rm d}$ converges. $Z_{\rm d}$ satisfies as the following relation

$$\begin{aligned} Z_{\rm d}^2 &= \sum_{m,n,k=0}^{\infty}P_{mnk}^2=\sum_{N=0}^{\infty}\sum_{m,n,k=0}^{N}\delta_{m+n+k,N}P_{mnk}^2 \\ &\leq \left(\sum_{N=0}^{\infty}\sum_{m,n,k=0}^{N}\delta_{m+n+k,N}|P_{mnk}|\right)^2 \\ &= \left[\sum_{N=0}^{\infty}\left(\frac{t_2+t_3+t_4}{t_1}\right)^N\right]^2. \end{aligned} \tag{38}$$

Therefore for $\frac{t_2+t_3+t_4}{t_1}<1$ the renormalization constant $Z_{\rm d}$ converges; the completly flat-band states appear.

Those two convergences for $Z_{\rm h}$ and $Z_{\rm d}$ agree with the previous sections, where we use the representations of the Bloch wavefunctions. However, we note that Eqs. (33)(38) give sufficient conditions for the convergence of the wavefunction. In Appendix A, we calculated

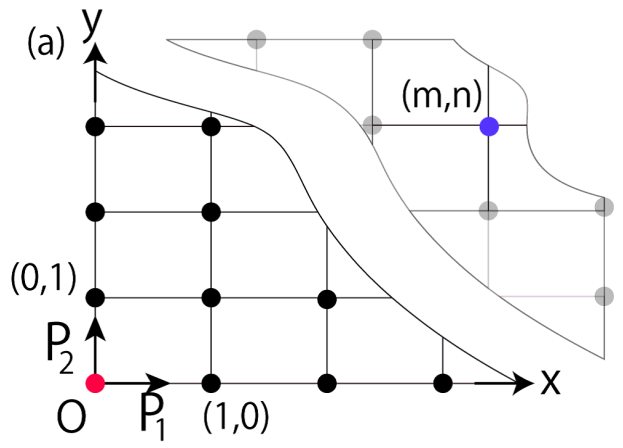

FIG. 9: Schematics of the grids for the shortest path problem. The mover is at first on the O, and it moves along $\mathbf{e}_i$ with the probability P_i, where $(\mathbf{e}_i)_j = \delta_{ij}$.

$Z_{\rm h}$ and $Z_{\rm d}$ for $t_1 = t$ and the others being unity, where t is the hopping parameter of the anisotropy. The results agree with the conditions in Eqs. (33)(38). From those results, we find that the edge/surface-localized wavefunctions spatially expand toward the interior of the systems, while the amplitude decays exponentially with the distance from the surface (Fig. 8).

VI. SUMMARY

Existence of flat-band boundary states is shown for tight-binding models on the diamond lattices. In the tight-binding model on the diamond-lattice model, we found that the distribution of the flat-band surface states at the Fermi energy is related with gapless loops in the bulk dispersion; the verge of the distribution of the flat bands in surface BZ is identical with the Fermi loop of the bulk projected on the surface direction. By increasing anisotropies of the hopping integrals, we showed that the distribution of the bulk Fermi surface shrinks and then disappears in the BZ. Then the surface flat band covers the surface BZ completely when the anisotropy is sufficiently large. In addition, we found a topological phase transition in the bulk Fermi loop in the tight-binding model on the diamond lattice by changing the anisotropy. These flat bands are understood topologically within the theory by Ryu and Hatsugai[8]. Lastly, for strongly anisotropic cases we constructed wavefunctions which is localized only on one site on the boundary layer. From the Schrödinger equation, we showed that the spatially localized flat-bands states exists in the honeycomb and diamond lattice models. The wavefunction is localized at a single site in the outermost edge/surface layer, while it expands inward with exponential decay.

In general, to obtain the localized boundary flat-band states, a bipartite lattice is necessary. Bipartite-lattice models can be made in several ways: for example, splitting the vertex of unipartite lattices. In addition when the system has anisotropy of the hopping integral along the direction normal to the surface, the boundary flat-bands appear. Thus to find candidate materials for the flat-band surface states, one need to find bipartite systems with strong anisotropy, and when the bulk is gapped, it may have the complete flat band depending on the surface orientation.

The flat bands discussed in this paper have different properties compared with the conventional flat bands[1–5]. Basically the conventional flat bands which cover the whole BZ originate from the difference of the numbers of the sublattices in the unit cell, while our system does not. Moreover, unlike those conventional flat-bands states, our flat-band states can be isolated from the bulk if the anisotropy becomes sufficiently large; in other words, the flat band is located in the middle of the bulk gap and the gap increases with the anisotropy. This property enables us to construct the fully localized boundary states.

Acknowledgments

This work is partially supported by the Global Center of Excellence Program by MEXT, Japan through the "Nanoscience and Quantum Physics" Project of the Tokyo Institute of Technology, Grant-in-Aid from MEXT, Japan (No. 21000004), JSPS Research Fellowships for Young Scientists, and TIES, Tokyo Institute of Technology. We thank H. Katsura, M. Ezawa, and S. Nakosai for useful discussions, and P. Delplace for notifying us us know of Ref. 11.

Appendix A: Calculations for normalization constants

In Appendix, we calculate the renormalization constants, $Z_{\rm h}$ and $Z_{\rm d}$ in Section V, for special cases where one of the hopping integrals is t and the others are unity. In the two cases, the hopping with t is perpendicular to the boundary.

1. Honeycomb lattice

For $t_1 = t \equiv x^{-1}$ and $t_2 = t_3 = 1$, $Z_{\rm h}$ is given as

$$\begin{aligned} Z_{\rm h}^2 &= \sum_{m,n=0}^{\infty} \left[\frac{(m+n)!}{m!n!} (-x)^{m+n} \right]^2 \\ &= \sum_{N=0}^{\infty} \sum_{m=0}^{N} \left[\frac{N!}{m!(N-m)!} \right]^2 x^{2N} \\ &= \sum_{N=0}^{\infty} \binom{2N}{N} x^{2N} = \frac{1}{\sqrt{1-4x^2}} \end{aligned} \tag{A1}$$

as long as $x = t^{-1}$ satisfies $|x| < \frac{1}{2}$. Therefore for $|t| > 2$ there are flat-band states which are localized on one site on the edge in the honeycomb lattice with zigzag edge.

2. Diamond lattice

For $t_1 = t$ and $t_2 = t_3 = t_4 = 1$, $Z_{\rm d}$ is given as

$$\begin{aligned} Z_{\rm d}^2 &= \sum_{m,n,k=0}^{\infty} \left(\frac{(n+m+k)!}{n!m!k!} \right)^2 t^{-2(n+m+k)} \\ &= \sum_{N=0}^{\infty} \sum_{m,k=0}^{\infty} \left(\frac{N!}{(N-m-k)!m!k!} \right)^2 t^{-2N} \\ &= \sum_{N=0}^{\infty} \oint_C \oint_C \frac{{\rm d}\xi {\rm d}\eta}{(2\pi i)^2 \xi\eta} (1+\xi+\eta)^N (1+\xi^{-1}+\eta^{-1})^N t^{-2N} \\ &= \oint_C \oint_C \frac{{\rm d}\xi {\rm d}\eta}{(2\pi i)^2 \xi\eta} \frac{1}{1-(1+\xi+\eta)(1+\xi^{-1}+\eta^{-1})Y^2} \quad \text{(A2)} \end{aligned}$$

where $t^{-1} = Y$ for notational brevity and we assume $0 \le Y \ll 1$. Later we can analytically continue the result with respect to Y to discuss the condition for convergence of $Z_{\rm d}$. ξ, η are complex numbers, and the path of the integrals are along the unit circle $C : |z| = 1$. In the above equation, by using $\xi = {\rm e}^{i\theta}$ and $\eta = {\rm e}^{i\phi}$ where $\theta, \phi \in \Re$, we have

$$\begin{aligned} Z_{\rm d}^2 &= \int_0^{2\pi} \frac{{\rm d}\theta {\rm d}\phi}{(2\pi)^2} \frac{1}{1-(1+{\rm e}^{i\theta}+{\rm e}^{i\phi})(1+{\rm e}^{-i\theta}+{\rm e}^{-i\phi})Y^2} \\ &= \int_0^{2\pi} \frac{{\rm d}\alpha {\rm d}\beta}{(2\pi)^2} \frac{1}{1-(1+4\cos^2\beta+4\cos\alpha\cos\beta)Y^2} \\ &= \frac{1}{2\pi Y^2} \int_0^{2\pi} \frac{{\rm d}\beta}{\sqrt{(4\cos^2\beta - p^2)(4\cos^2\beta - q^2)}}, \quad \text{(A3)} \end{aligned}$$

where $\alpha = \frac{\theta+\phi}{2}$, $\beta = \frac{\theta-\phi}{2}$, $p = 1 + \frac{1}{Y}$, $q = \frac{1}{Y} - 1$, and we use the relation $\int_0^{2\pi} {\rm d}\alpha \frac{1}{A+B\cos\alpha} = \frac{{\rm sgn}(A)}{\sqrt{A^2-B^2}}$ for $|A| > |B|$, and $A, B \in \Re$. By changing the variable as $\tan\beta = v$, the above equation becomes

$$Z_{\rm d}^2 = \frac{2}{\pi Y^2 pq} \int_0^{\infty} {\rm d}v \frac{1}{\sqrt{(v^2+b^2)(v^2+c^2)}}, \quad \text{(A4)}$$

where $b^2 = 1 - \frac{4}{q^2}$ and $c^2 = 1 - \frac{4}{p^2}$. The integral is further transformed to the elliptic integral of the first kind,

$$Z_{\rm d}^2 = C(Y) \int_0^1 \frac{{\rm d}s}{\sqrt{(1-s^2)(1-k^2s^2)}}, \quad \text{(A5)}$$

$$C(Y) = \frac{2}{\pi Y^2 pqc} = \frac{2}{\pi\sqrt{(1-Y)^3(1+3Y)}}, \quad \text{(A6)}$$

$$k^2 = \frac{16Y^3}{(1-Y)^3(3Y+1)}, \quad \text{(A7)}$$

where the variable is changed as $v = \frac{bs}{\sqrt{1-s^2}}$. By the above result, for $0 \le Y < \frac{1}{3}$, k^2 satisfies $0 \le k^2 < 1$, and $Z_{\rm d}^2$ converges. On the other hand, for $Y < 0$, because $Z_{\rm d}^2$ is an even function of Y, $Z_{\rm d}^2$ converges for $-\frac{1}{3} < Y < 0$. Namely, the condition for the convergence of the normalization constant $Z_{\rm d}$ is $|t| < 3$.

[1] E. H. Lieb, Phys. Rev. Lett. **62**, 1201 (1989).
[2] A. Mielke, J. Phys. A: Math. Gen. **24**, L73 (1991).
[3] A. Mielke, J. Phys. A **24**, 3311 (1991).
[4] A. Mielke, J. Phys. A **25**, 4335 (1992).
[5] A. Mielke and H. Tasaki, Commun. Math. Phys. **158**, 341 (1993).
[6] K. S. Novoselov *et al.*, Science **306**, 666 (2004).
[7] M. Fujita *et al.*, J. Phys. Soc. Jpn. **65**, 1920 (1996).
[8] S. Ryu, Y. Hatsugai, Phys. Rev. Lett. **89**, 077002 (2002).
[9] Y. Takagi and S. Okada, Surf. Sci. **602**, 2876 (2008).
[10] P. Dietl, F. Piechon, G. Montambaux, Phys. Rev. Lett. **100**, 236405 (2008).
[11] P. Delplace , D. Ullmo, G. Montambaux, Phys. Rev. B **84**, 195452 (2011).
[12] M. Kohmoto and Y. Hasegawa, Phys. Rev. B **76**, 205402 (2007).